Everyone works better together: rational improvements to radio- and immunotherapy combinations

Frijlink, E.S.

4

Radiotherapy and Cisplatin increase immunotherapy efficacy by enabling local and systemic intratumoral T-cell activity

Cancer Immunology Research. 2019;7(4): 670-682

Paula Kroon[1*], **Elselien Frijlink**[1*], Victoria Iglesias-Guimarais[1], Andriy Volkov[1], Marit M. van Buuren[1], Ton N. Schumacher[1,2], Marcel Verheij[3], Jannie Borst[1#], and Inge Verbrugge[1#]

[*] *Shared first authors*
[#] *Shared senior authors*
[1]Division of Tumor Biology and Immunology, The Netherlands Cancer Institute-Antoni van Leeuwenhoek, 1066 CX Amsterdam, The Netherlands.
[2]Division of Molecular Oncology and Immunology, Oncode Institute, The Netherlands Cancer Institute-Antoni van Leeuwenhoek, 1066 CX Amsterdam, The Netherlands.[3]Department of Radiation Oncology, The Netherlands Cancer Institute-Antoni van Leeuwenhoek, 1066 CX Amsterdam, The Netherlands.

Abstract

To increase cancer immunotherapy (IT) success, PD-1 blockade must be combined with rationally selected treatments. Here, we examined, in a poorly immunogenic mouse breast cancer model, the potential of antibody-based immunomodulation and conventional anticancer treatments to collaborate with anti-PD-1 treatment. One requirement to improve anti-PD-1-mediated tumor control was to promote tumor- specific cytotoxic T-cell (CTL) priming, which was achieved by stimulating the CD137 costimulatory receptor. A second requirement was to overrule PD-1-unrelated mechanisms of CTL suppression in the tumor microenvironment (TME). This was achieved by radiotherapy (RT) and cisplatin treatment. In the context of CD137/PD-1-targeting IT, RT allowed for tumor elimination by altering the TME, rather than intrinsic CTL functionality. Combining this radioimmunotherapy regimen with low-dose cisplatin improved CTL-dependent regression of a contralateral tumor outside the radiation field. Thus, systemic tumor control may be achieved by combining IT protocols that promote T-cell priming with (chemo)radiation protocols that permit CTL activity in both the irradiated tumor and (occult) metastases.

Running title

Chemo-radio-immunotherapy in PD-1 resistant breast cancer.

Introduction

Cancer immunotherapies include adoptive T-cell therapy, therapeutic vaccination, and/or antibody-based immunomodulation. From a technical perspective, antibody-based immunomodulation is relatively straightforward, because immunomodulatory antibodies can essentially be delivered in the same way as conventional anticancer drugs. Immunomodulatory antibodies approved for cancer immunotherapy (IT) are designed to target the T-cell coinhibitory receptors PD-1 or CTLA-4, and single or combined treatment induces durable responses in about one third of patients with solid tumors[1]. Still, the majority of patients do not benefit from this treatment approach[2]. Compared with targeting CTLA-4, targeting PD-1 is generally more successful and associated with fewer autoimmune symptoms[3]. Therefore, targeting PD-1 currently serves as the backbone for developing new combination therapies. To choose combinations rationally, insight into their combined mechanism of action is required.

$CD8^+$ cytotoxic T lymphocytes (CTL) can recognize (tumor-derived) intracellular peptides presented on the cell surface by MHC class I molecules. As MHC class I molecules are expressed on virtually all body cells, CTLs can in principle target any cancer type. $CD4^+$ T cells also promote antitumor immunity, either by direct cytotoxic activity or by promoting the activity of CTLs and other immune cells[4]. Several groups postulated that successful IT relies on a tumor-specific T-cell response that is self-sustained by continuous generation of new effector T cells (T cell priming) and support of their activity[5,6]. To enable this cycle, the tumor must essentially act as its own 'vaccine' by releasing both recognizable antigens and 'danger' signals. Dendritic cells (DCs) can then present these antigens to naïve T cells and provide appropriate costimulatory and cytokine signals needed to induce T cell clonal expansion and effector differentiation. However, in immunogenic tumors that have given rise to a T-cell response throughout their development, negative feedback mechanisms reduce effector T-cell functions. These mechanisms include the activity of regulatory T cells (Tregs) and suppressive activity of myeloid cells, stromal cells, and even the tumor cells themselves[7]. For example, PD-L1 can be expressed on tumor cells and/or other (immune) cell types present in the tumor, and can inhibit T-cell function via PD-1[8]. Successful IT requires the elimination of such suppressive mechanisms.

Blocking CTLA-4 enables CD28 costimulation[9], which may promote new T-cell priming and effector T-cell activity. Blocking CTLA-4 and PD-1 promotes T-cell activity inside tumors in a complementary fashion[10] and blocking CTLA-4 promotes T-cell priming in patients with cancer[11]. Concomitant targeting of CTLA-4 and PD-1 is associated with increased autoimmunity[12] and this combination should likely be avoided when developing new IT strategies. A potential alternative, targeting CD137 (also known as 4-1BB or TNFRSF9) using agonistic antibodies is currently in phase III clinical trials[13] and is being tested in combination with PD-1 blockade in phase 1b clinical trials[14]. CD137 is

a costimulatory receptor that belongs to the Tumor Necrosis Factor (TNF) receptor family, and its signaling promotes the priming and maintenance of CTL responses by delivering prosurvival and other signals to $CD8^+$ T cells and DCs[15].

Both radiotherapy (RT) and chemotherapy induce tumor cell destruction, which leads to release of antigens and 'danger' signals[16]. In principle, these events may lead to new T-cell priming. However, the likelihood that priming will occur without IT-based assistance is low, because RT almost never gives rise to an 'abscopal' effect, i.e. regression of a tumor mass outside the radiation field[17]. Extrapolating from mouse models[18], conventional chemotherapeutic drugs may have immunomodulatory actions in human, but thus far, this question has not been a systemically address in the clinic.

Here, we examined the potential of using RT and a routinely co-applied conventional chemotherapy (cisplatin) to assist IT in evoking a systemic, tumor-eradicating T-cell response. We provide evidence that RT and chemotherapy make tumors permissive to CTL activity. These data argue that conventional anticancer regimens can be combined rationally with IT to improve systemic tumor control and increase tumor clearance rates and patient outcome.

Results

Immunotherapy (IT) with CD137 agonism and PD-1 blockade promotes T-cell priming

As a model system, we used mice with syngeneic AT-3 breast cancer cells implanted orthotopically into the fat pad and treated with IT and/or RT after the tumor reached $>20mm^2$. Standard IT consisted of a blocking antibody to PD-1 and an agonistic antibody to CD137 (Figure **1A**), targets which are expressed on DCs and on T cells in lymphoid organs and tumor tissue (Figure **S1**). In this setting, IT and RT as individual treatments merely delayed tumor outgrowth, whereas combined treatment (i.e. RIT) resulted in tumor clearance in the majority of the mice (Figure **1B**). We have previously shown that combined PD-1 blockade and CD137 agonism is more effective at enhancing RT-induced tumor control than single PD-1 blockade or CD137 agonism and that tumor control in this setting relies on $CD8^+$ T cells[19,20].

Among single modality treatments, CD137 agonism, but not RT or PD-1 blockade induced a T-cell response (Figure **1C**), as determined by the appearance of $CD4^+$ and $CD8^+$ T cells with a $CD43^+$ effector phenotype in blood posttreatment[21]. PD-1 blockade further increased $CD4^+$ and $CD8^+$ T-cell responses when combined with CD137 agonism (Figure **1C,D**). Finally, when IT with both antibodies was combined with RT, $CD4^+$ and $CD8^+$ T-cell responses were also induced, as measured by a significant increase in effector phenotype T cells in the blood and a similar increase in the

(inguinal) tumor-draining lymph node (dLN) (Figure **1D,E**). These data suggest that IT with CD137 agonist antibody promotes T-cell priming, which is increased by PD-1 blockade and not impeded by concurrent RT.

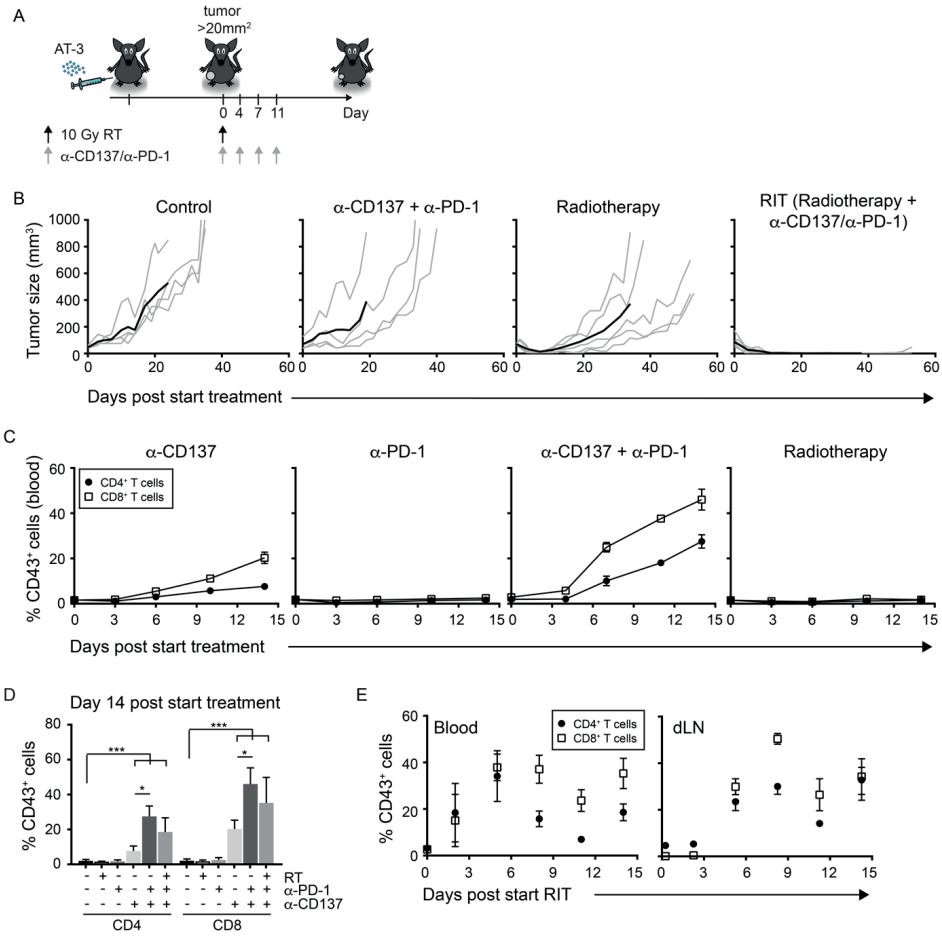

Figure 1. Immunotherapy with CD137 agonism and PD-1 blockade promotes T-cell priming.
(**A**) Experimental set-up. (**B**) Tumor growth curves measured in mice receiving the indicated therapies (n=4–5/group). Gray lines, individual mice; black line, group average. (**C**) CD43 expression on $CD4^+$ and $CD8^+$ T cells in blood, in tumor- bearing mice (n=5/group) at indicated time points posttherapy. (**D**) Pooled data (mean +SD) from **C** and **E**, showing the frequency of effector phenotype T cells in blood on day 14 side-by-side. (**E**) CD43 expression on $CD4^+$ and $CD8^+$ T cells, in the blood (left) and draining lymph node (dLN) of tumor-bearing mice (n=4–5/group), at different time points after RIT (* , $P < 0.01$; ***, $P < 0.001$).

Control of the irradiated tumor by radio-immunotherapy (RIT) requires T-cell priming

To examine whether newly primed T cells contributed to tumor control after RIT, we treated mice with the drug FTY720 that induces the internalization of the sphingosine 1 phosphate receptor 1 (S1PR1). T cells use the S1PR1 to egress from secondary lymphoid organs and the drug prevents them from doing so[22]. RIT was applied while the mice were treated with FTY720 or vehicle (Figure **2A**, Figure **S2A**). To assess T-cell priming and resulting effector T-cell generation, we measured the percentage of $CD4^+$ and $CD8^+$ T cells in the dLN that could produce the effector cytokines TNFα and/or IFNγ. RIT increased the percentage of $CD8^+$ effector T cells, and these cells significantly accumulated in the dLN upon FTY720 treatment (Figure **2B**, left). In contrast, TNFα-producing $CD4^+$ effector T cells were not increased by RIT, nor did these cells accumulate in the dLN upon FTY720 treatment (Figure **2B**, right). These data indicate that RIT induced new priming of $CD8^+$ T cells and that FTY720 treatment effectively 'trapped' these newly primed T cells in the dLN.

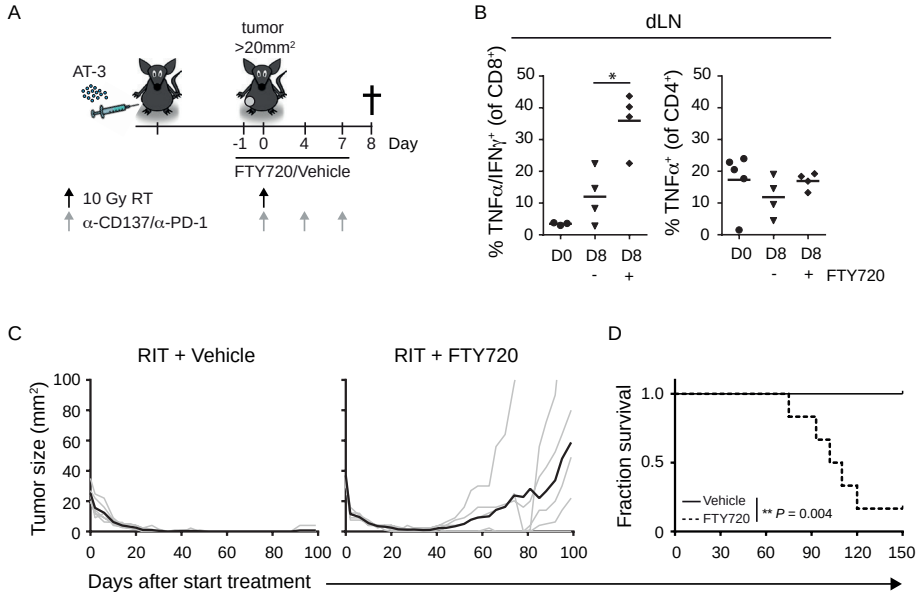

Figure 2. Control of the irradiated tumor by RIT requires T-cell priming.
(**A**) Experimental set-up for **B**. (**B**) Percentage of $CD4^+$ (right) and $CD8^+$ T cells (left) in the dLN that produce TNFα/IFNγ or TNFα in response to *in vitro* restimulation, before (D0, closed circles) or 8 days (D8) after starting RIT, in presence (closed diamonds) or absence (closed triangles) of FTY720 (* , $P < 0.05$). Tumor growth (**C**) and survival curves (**D**) of AT-3 tumor-bearing mice (n=6/group) receiving RIT with FTY720 or vehicle.

Whereas 100% of the mice cleared their tumor and survived long term upon RIT, concurrent FTY720 treatment significantly increased tumor outgrowth (Figure **2C**) and reduced overall survival (Figure **2D**). FTY720 treatment did not reduce the therapeutic effect of RT or IT alone (Figure **S2B**). Thus, RIT leads to T-cell priming and these newly primed T cells make a critical contribution to regression of the irradiated tumor.

RIT does not induce regression of an abscopal tumor, despite infiltration with newly primed CTLs

Given that RIT induces T-cell priming, we hypothesized that the resulting systemic T-cell response could also act against a nonirradiated tumor in the same host. We tested this by implanting two tumors into the same mouse; one in the left fat pad and the other in the contralateral flank. Only the latter tumor was irradiated (Figure **3A**). The T-cell response and tumor regression were examined for both tumors.

We found that after RIT the percentage of $CD8^+$ T cells among total $CD45^+$ (hematopoietic) cells increased significantly in both irradiated and nonirradiated tumors (Figure **3B**, right). The RIT-induced increase of $CD8^+$ T cells in the nonirradiated tumor was largely prevented by FTY720 treatment (Figure **3B**, right), indicating that this increase was largely due to new T-cell priming. The $CD4^+$ T-cell response following RIT was much less pronounced (Figure **3B**). Histologic analysis confirmed that $CD8^+$

T cells accumulated to a similar extent following RIT in both irradiated and nonirradiated tumors (Figure **3C**). Infiltration by CTLs, capable of producing IFNγ and TNFα and the cytotoxic effector molecule Granzyme B, was of similar magnitude in irradiated and nonirradiated tumors (Figure **3D**). In contrast, accumulation of $CD4^+$ T cells that could produce TNFα or Granzyme B was not evident (Figure **3E**). As compared with IT alone, RIT delayed outgrowth of the irradiated tumor, but not of the nonirradiated tumor (Figure **3F**, Figure **S3A**). As overall survival was defined by the time for any the two tumors to reach 100 mm^2, RIT did not improve overall survival of mice as compared with IT alone (Figure **3G**). (Hypo)fractionated RT is more effective than single-dose RT in enhancing abscopal tumor control by IT in certain mouse models[23,24]. However, 3 x 8 Gy (hypo)fractionation also did not enhance IT-induced control of nonirradiated AT-3 tumors (Figure **S3B, C**). Thus, CTLs that are raised by RIT are present in equal measure in the irradiated and nonirradiated tumor, yet these CTLs can only eliminate the irradiated tumor.

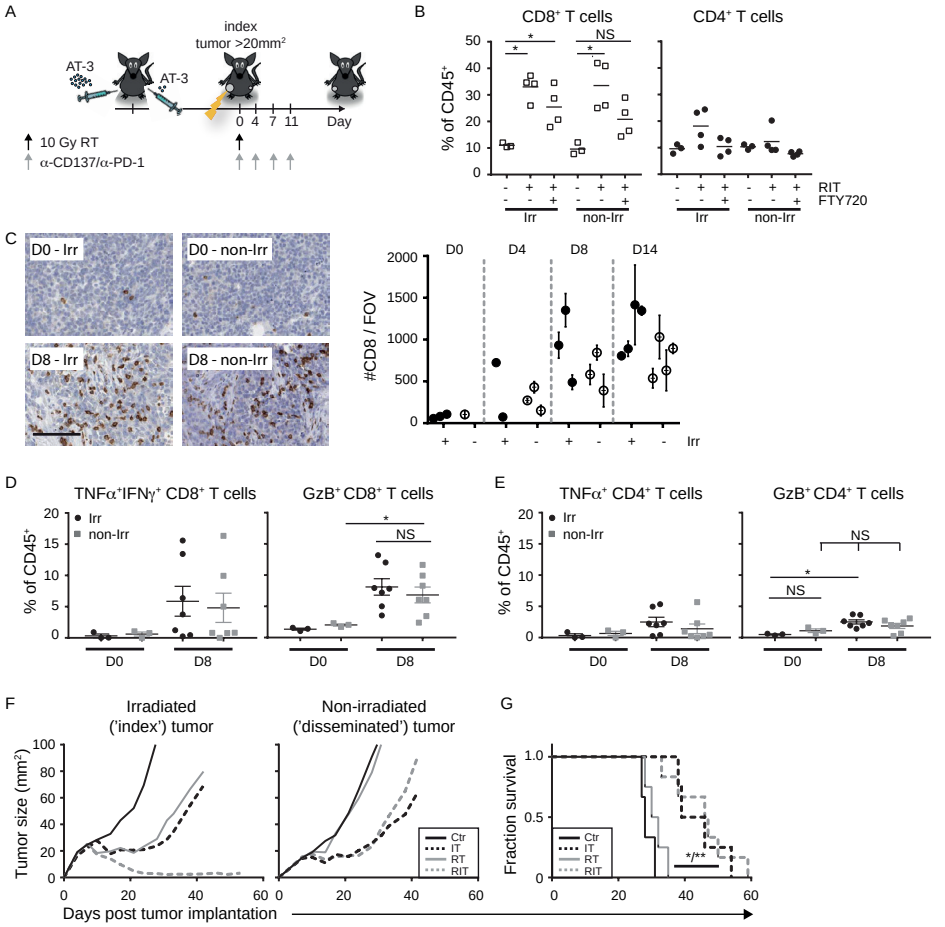

Figure 3. RIT leads to comparable infiltration of irradiated and nonirradiated tumors with T cells, but the nonirradiated tumor does not regress.

(**A**) Experimental set-up. (**B**) Percentage of $CD4^+$ and $CD8^+$ T cells within the $CD45^+$ cell population in the irradiated (Irr) and nonirradiated (non-Irr) tumors before (-) or 8 days after the start of RIT, in the presence or absence of FTY720. * $P < 0.05$. C, AT-3 tumor sections (n=3 mice/group) were stained for CD8 before treatment (D0) or 4, 8, or 14 days after the start of RIT. Left:, representative images; right, summary data. Quantification in the right represents the average (SD) of 5 fields of view (FOVs) for 3 irradiated (filled circles) and 3 nonirradiated tumors (open circles). Images represent 1/6th of a FOV; scale bar, 100 mm. (**D**, **E**) Percentage of $TNF\alpha^+IFN\gamma^+$ or Granzyme B $(GzB)^+$ $CD8^+$ T cells (**D**) and $CD4^+$ T cells (**E**) within the $CD45^+$ cell population isolated from irradiated and nonirradiated tumors before (D0) and 8 days after starting RIT. Each symbol represents a single tumor, and the mean is indicated.* , $P < 0.05$. (**F**) Mean tumor growth in mice (n=5–6/group) that received no therapy (Ctr), RT (10 Gy, R), alone or in combination with IT. (**G**) Survival curve for mice treated as indicated. *, $P < 0.05$, between the Ctr and IT groups; **, $P < 0.01$ between the Ctr and RIT groups and between the RT and RIT groups.

The abscopal effect of RIT is not limited by T cell priming, intratumoral neutrophils/macrophages

We next addressed a number of potential factors that might prevent RIT-induced CTLs from eliminating the nonirradiated tumor. We first assessed whether the size of the tumor-specific effector CTL pool was a limiting factor. For this purpose, we identified the peptide SNPTYSVM from MMTV-Polyoma virus middle-T (PyMT) as an MHC class I-restricted antigen that could raise T-cell immunity to AT-3 tumor cells (Figure **S4A-F**). This enabled us to purposely generate tumor-specific CTL memory *in vivo* by vaccinating mice with plasmid (p)DNA encoding this epitope (Figure **4A**), designed according to ref[25]. Vaccinated mice were challenged with two AT-3 tumors and treated with RIT (Figure **4B**). Also, in this setting, RIT did not enhance control of the nonirradiated tumor (Figure **4C**) or improve survival of mice (Figure **4D**), as compared with IT alone. These data suggest that the magnitude of the tumor-specific CTL response was not the limiting factor for systemic tumor control following RIT.

We next examined which mechanisms of T-cell suppression other than PD-1/PD-L1 interaction may operate in the nonirradiated AT-3 tumors. Treg frequency was low in the irradiated and nonirradiated tumors and did not change significantly following RIT (Figure **4E**), suggesting that it did not correlate with CTL-mediated tumor control.

Tumor-resident neutrophils and macrophages can also locally impair CTL function[26]. Following RIT, a decrease in the frequency of $F4/80^{+}MHCII^{+}$ TAMs was observed in irradiated, but not in nonirradiated tumors (Figure **4F**, left). The frequency of $Ly6G^{+}Ly6C^{low}$ neutrophils did not change after RIT (Figure **4F**, right). In addition, antibody-mediated depletion of neutrophils or TAMs (Figure **S4G**) did not improve control of nonirradiated tumors (Figure **S4H**), nor did it increase overall survival following RIT (Figure **4G**).

Following RIT, the frequency of NK cells and NK-T cells was decreased in irradiated and nonirradiated tumors to a similar extent. There was also no difference in the frequency of $Ly6C^{hi}Ly6G^{-}$ inflammatory monocytes, $CD103^{+}$ DCs, and $CD11b^{+}$ DCs in irradiated as compared to nonirradiated tumors (Figure **4H**). Thus, the presence of these cell types did not correlate with CTL-mediated tumor control.

Although RT can upregulate cell surface expression of MHC class I[27], it did not increase MHC class I expression on nonhematopoietic cells in the AT-3 tumor *in vivo*, as determined on day 3 and 8 post RT (Figure **S4I**). Taken together, these data suggest that the magnitude of the tumor-specific CTL response, PD-1 signaling, Tregs, neutrophils, TAMs, NK(T) cells, inflammatory monocytes, DCs, or MHC class I expression were not key factors that limited CTL activity in the nonirradiated tumor after RIT.

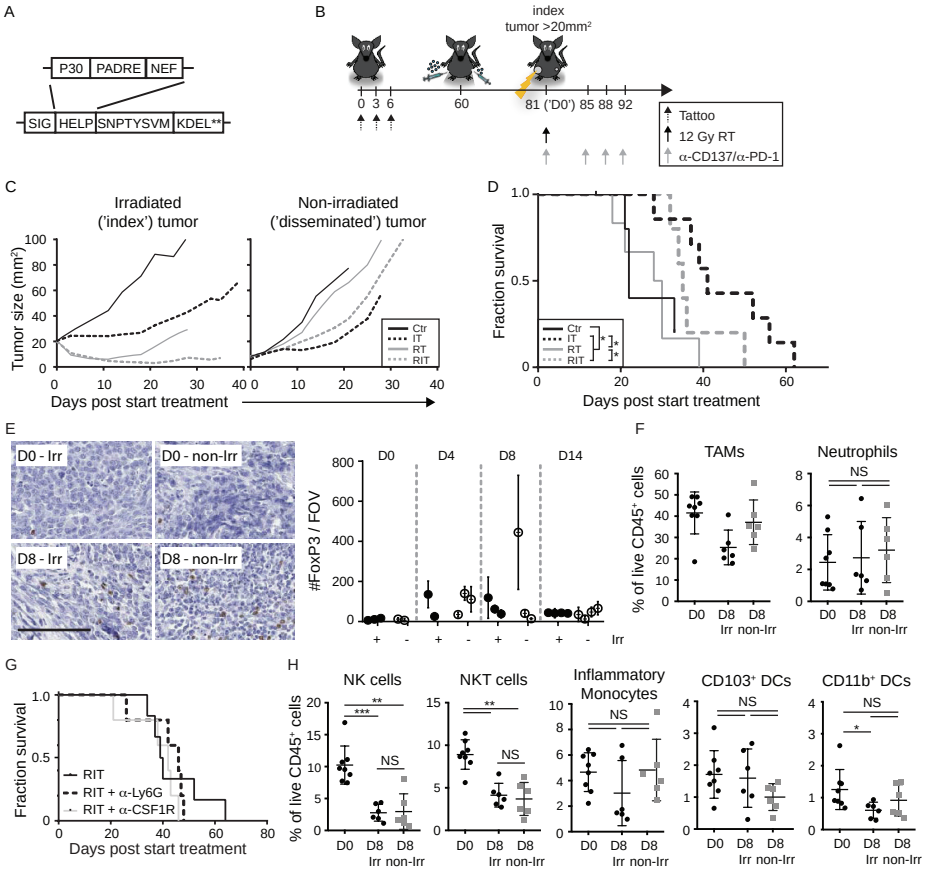

Figure 4. Optimizing tumor-specific T-cell priming, depletion of neutrophils or TAMs is insufficient to control nonirradiated AT-3 tumors following RIT.

(**A**) The vaccine encodes the H-2K^{b}-binding PyMT epitope SNPTYSVM and MHC II "helper" epitopes. **, Double stop codon. (**B**) Experimental set-up. Mean tumor size (**C**) and survival curves (**D**) of 5–7 mice/group that received the indicated treatments. *, P < 0.05. (**E**) FoxP3^{+} regulatory T cells in irradiated (Irr) and nonirradiated (non-Irr) tumors before treatment (D0) and on the indicated days after the start of RIT (n=3/group). Images, representative FoxP3 staining of 10% of a FOV; scale bar, 100 mm. Quantification (right): mean (SD) of 5 FOVs for 3 irradiated (filled circles) and 3 nonirradiated tumors (open circles). (**F,H**) TAMs, neutrophils (**F**), NK cells, NKT cells, inflammatory monocytes, CD103^{+} DCs, CD11b^{+} DCs (**H**) in untreated (D0), irradiated (irr), and nonirradiated (non-irr) tumors on day 8 (D8) after RIT. Each symbol represents an individual tumor, and the mean (SD) is shown (*, P < 0.05; **, P < 0.01; *** , P < 0.001). (**G**) Survival curve of tumor-bearing mice that receive RIT in the presence or absence of antibodies targeting Ly6G or CSF1R (n=5/group).

RIT induces a TME characterized by reduced cell proliferation and increased tissue repair

RIT led to the same degree of CTL infiltration in the irradiated and nonirradiated tumors, whereas only the irradiated tumor regressed, suggesting that CTLs can exert their activity on tumor cells only after the tumor has been altered by irradiation. To understand the immunomodulatory effect of irradiation in the context of IT, we performed mRNA sequencing (RNA-seq). Eight days after RIT (allowing sufficient time for T cells to infiltrate both tumors: see Figure **3**), we sorted the effector ($CD43^+$) $CD8^+$ T cells (i.e. 'CTLs'), $CD45^+$ hematopoietic cells (excluding $CD43^+CD8^+$ T cells) and $CD45^-$ tumor/stromal cells (Figure **5A**). Statistical analysis of normalized read counts revealed the differential expression of 805 genes in CTLs (Figure **5B**), 1107 genes in the hematopoietic cells (Figure **5C**), and 3045 genes in the tumor/stromal cells (Figure **5D**). These genes encode a wide diversity of proteins (Table **S1**) that perform a multitude of cellular functions.

We identified groups of biological processes that were differentially modulated between the cell populations at the irradiated and nonirradiated tumor sites. In all three cell populations, gene sets associated with cell division, DNA replication and repair, and chromatin remodeling were significantly downregulated in the irradiated tumor (Figure **5E-G**), congruent with the cells receiving a DNA-damaging input in the form of irradiation.

In the CTLs, we additionally identified a small group of gene sets associated with negative regulation of cytokine expression (Figure **5E**), that included both *Foxp3* and *Il10* (Table **S1**), which may report effects of irradiation. We did not identify gene sets associated with increased CTL-intrinsic effector function that could explain the increased CTL efficacy in the irradiated tumor. This finding is consistent with our functional data regarding $CD8^+$ T cells, showing that both irradiated and non-irradiated tumors are infiltrated with effector-phenotype CTLs after RIT (see Figure **3D**).

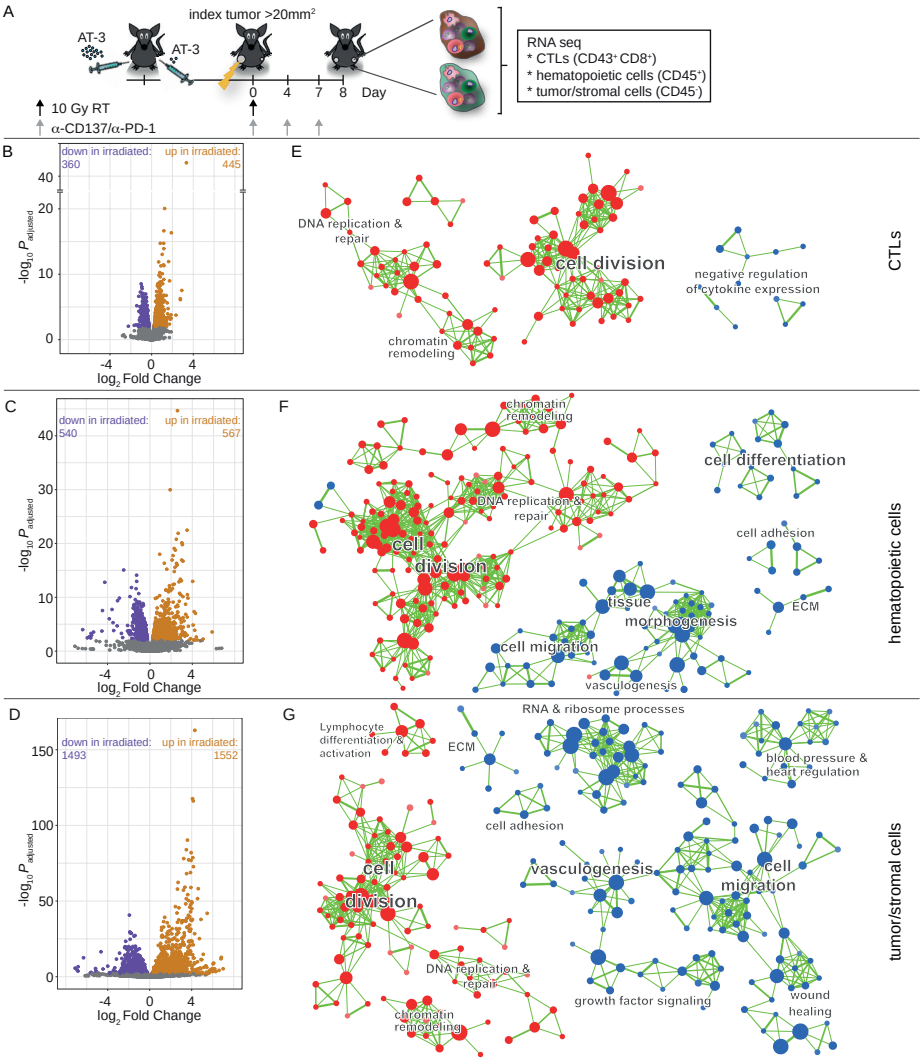

Figure 5. RIT induces a CTL-permissive TME that is characterized by gene signatures associated with reduced cell proliferation and increased response to tissue injury.
(**A**) Experimental set-up. (**B–D**) Volcano plots of the indicated cell populations showing significant (adjusted P < 0.01) transcriptomic changes in the irradiated compared with the nonirradiated tumor. Purple, orange, and gray dots represent downregulated, upregulated, or unchanged genes, respectively. (**E–G**) Enrichment Maps showing significantly enriched gene sets (biological processes) in blue (enriched in the irradiated tumor) and red (enriched in the nonirradiated tumor). Gene sets that share a high number of genes are clustered together, and the thickness of the green lines represents the number of shared genes. Clusters of similar biological processes are labeled.

In the hematopoietic and tumor/stromal cells, we identified several biological processes that were significantly different between the irradiated and nonirradiated tumor sites (Figure **5F** and **G**). These included overlapping processes and genes in the hematopoietic and tumor/stromal cells, such as increased cell migration e.g. *Cxcl17*, *Cxcl14*), vasculogenesis (e.g. *Vegfc*, *Egfl7I)*, and cell adhesion/extracellular matrix (ECM; e.g. *Selp*, *Mmp3*, see also Table **S1**). In addition, and unique to the tumor/stromal cell population, we identified increased expression of gene sets associated with RNA/ribosome processes (e.g.*Rps19*, *Rps12*) and wound healing (e.g. *Pdgfb*, *Cxcl12*) in the irradiated tumor as compared to the nonirradiated tumor (Figure **5F, G**). Increased expression of proapoptotic *Bax* was observed specifically in the tumor/stromal cells of the irradiated tumor (Table **S1**).

Taken together, these RNA-seq data revealed that the TME of the irradiated tumor was different from that of the nonirradiated tumor. RT inflicted a DNA damage response in all cell populations in the tumor and led to tissue repair, as suggested by increased protein translation, angiogenesis and cell migration. This gene expression profile was associated with increased CTL activity against the tumor cells, most likely through CTL-extrinsic effects.

Cisplatin functionally mimics the RT-induced, T cell permissive TME and increases RIT efficacy

Next, we aimed to create a 'CTL-permissive' TME in the nonirradiated tumor to allow for systemic CTL-based tumor eradication following RIT. We tested low-dose cisplatin chemotherapy to achieve this effect (Figure **6A**) for the following reasons: *i*) Cisplatin has partially the same mode of action as RT by inducing DNA damage, *ii*) cisplatin combined with RT is standard-of-care in the treatment of different types of cancer and *iii*) (low-dose) cisplatin has been shown to support T-cell function in (pre-)clinical vaccination studies[18].

We found that low-dose cisplatin delayed tumor outgrowth, and that adding cisplatin treatment to RIT further improved control of nonirradiated tumors (Figure **6B** and **C**) and increased overall survival (Figure **6D**). This enhanced therapeutic effect was $CD8^+$ T-cell-dependent (Figure **6D**), even though cisplatin modestly reduced the magnitude of the T-cell response following RIT (Figure **S5A** and **S5B**). In the absence of RT, cisplatin treatment also enhanced the antitumor effect of this IT approach (Figure **S5C** and **S5D**). Thus, systemic cisplatin treatment functionally mimicked the localized effects of RT, allowing CTL-mediated growth delay of the non-irradiated tumor and prolonging overall survival following RIT.

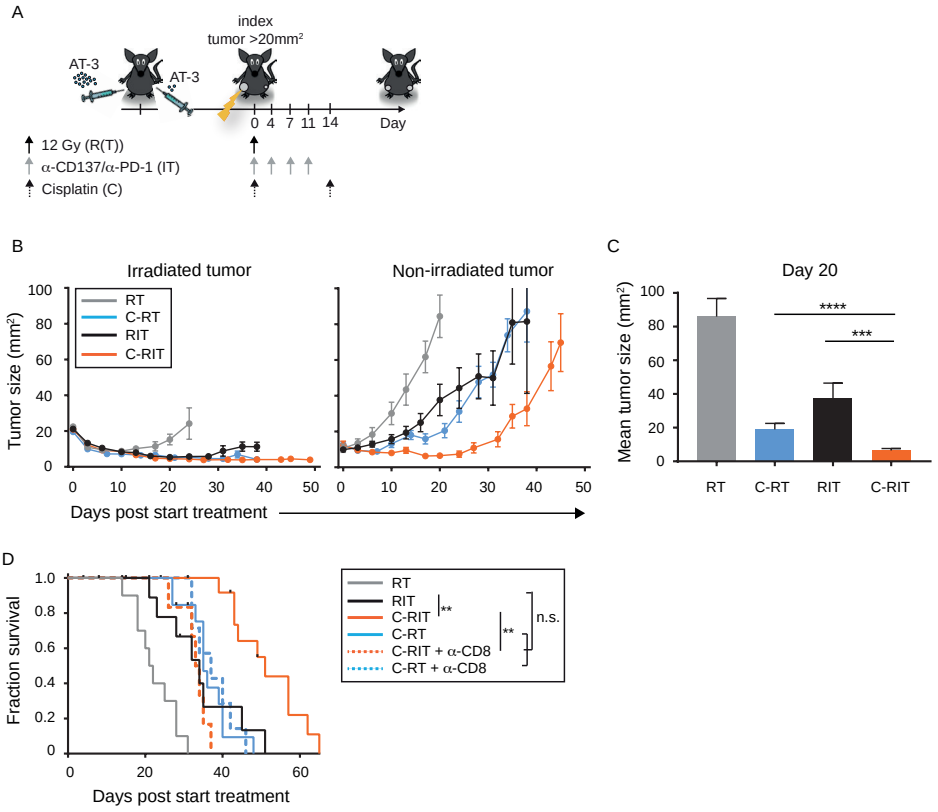

Figure 6. Cisplatin increases the therapeutic efficacy of RIT.

(**A**) Experimental set-up. (**B**) Mean tumor growth (SEM) of irradiated and nonirradiated tumors. Mean tumor size (± SEM) of nonirradiated tumors on day 20 (**C**) and survival curves of the indicated groups of mice; where indicated a CD8-depleting antibody (α-CD8) was administered one day before the start of treatment (**D**). Data shown are pooled data from 3 independent experiments of 4–7 mice/group in each experiment. ** P < 0.01; ***, P < 0.001; ****, P < 0.0001; n.s., not significant.

Discussion

There is an unmet clinical need to improve responses to PD-1 blockade, which currently forms the backbone for IT combinations[2]. The PD-1 coinhibitory receptor is associated with tyrosine phosphatase activity that inhibits CD3/CD28 signalling[8]. In this way, the PD-1 'checkpoint' can impede both T-cell priming and effector function. In patients with cancer, PD-1 blockade thus far seems to primarily relieve effector T cells from PD-L1/2-based suppression in the TME[28]. Therefore, this approach is likely to be most effective as standalone treatment for immunogenic cancers in which T cells have already infiltrated the tumor[29]. IT of poorly immunogenic cancers that have not raised a T-cell response will by definition require interventions that induce tumor-specific T-cell priming. Even in immunogenic cancers that respond to PD-1 blockade alone, new T-cell priming

is expected to strengthen and broaden the anti-tumor immune response, thereby increasing efficacy and combatting resistance[6]. In addition, immune suppression within the TME will preexist in immunogenic tumors and may develop in poorly immunogenic tumors once a T-cell response is raised, resulting from negative feedback control. PD-1/PD-L1 interactions are only a small part of this feedback control, which is exerted by diverse immune- and nonimmune cells in the TME. Effective antitumor immunity requires both priming of tumor-specific T-cells and a CTL-permissive TME. Here, we show that RT and conventional chemotherapy can promote intratumoral CTL activity by modulating the TME and by synergizing with an IT that enables T-cell priming.

We here identified that the murine AT-3 breast cancer cell line carries a foreign antigen MHC class I-restricted antigen 'SNPTYSVM'. Few T cells were present within AT-3 tumors at steady-state. PD-1 blockade alone had no therapeutic effect, but CD137 agonism induced CTL priming and anti-tumor immunity. CD137 triggering on activated $CD8^+$ T cells stimulates proliferation, survival and possibly effector differentiation[15], supporting CTL priming. Furthermore, CD137 triggering on DCs and other myeloid cell types can lead to the upregulation of costimulatory ligands CD80/CD86 (e.g.[30]), which may help to overcome peripheral tolerance and induce T-cell responses to tumor antigens. In the TME, CD137 agonism may support CTL function by similar mechanisms. CD137 mAb can also stimulate hypoxic, CD137-expressing endothelial cells to recruit T cells into the tumor[31]. We found that PD-1 blockade aided CD137-stimulated CTL priming, supporting evidence that the PD-1 checkpoint can also limit T-cell priming, as observed previously (e.g.[32]).

We predict that combining PD-1 blockade with any form of immunomodulation that induces CTL priming will be generally useful clinically. CTLA-4 blockade (e.g.[24]) and CD27 agonism[33] can exert similar effects in distinct tumor models. In our current study and previous ones[19,20,34], agonistic antibody to CD137 administered either intratumorally or intraperitoneally, did not lead to weight loss or other overt pathology of the mice in the context of RIT. In humans, in which CD137 agonist antibody is applied systemically, combination with PD-1 blockade has comparable side-effects as PD-1 blockade alone, suggesting the approach is feasible[14].

In the IT setting with combined PD-1 blockade and CD137 agonism, AT-3 tumors were not eliminated, despite a robust CTL response. In adoptive tumor-specific T-cell therapy, a robust CTL response is often also not sufficient for tumor control[35], highlighting that CTL suppression in the TME can pose an additional bottleneck for systemic antitumor immunity. Our study demonstrates that RT can alter the state of the TME to permit effective CTL activity, under conditions where PD-1 blockade cannot. Newly primed CTLs raised by our RIT protocol contributed to control of the irradiated tumor. Having a second, nonirradiated tumor in the same mouse allowed us to pinpoint the immune modulating effects of RT. The nonirradiated tumor was similarly infiltrated by newly primed CTLs as the irradiated tumor, but did not regress, indicating that impediments beyond

PD-1 signaling hampered abscopal tumor control. In a CT26 transplantable tumor model, control of the irradiated tumor by combined RT and PD-1 blockade was also found to be partly dependent on newly primed T cells. In that model, control of a simultaneously implanted nonirradiated tumor was also improved by PD-1 blockade[36]. In that case, PD-1 signaling was the key impediment for CTL activity in the TME, whereas in our AT-3 model, additional impediments were in place. In PyMT-induced tumors, stimulation of TAMs with TLR7/9 agonists (imiquimod, CpG) allowed them to reactivate tumor-resident T cells[37]. However, in the AT-3 model, the CTL-enabling effect of RT could not be reproduced by depletion of neutrophils or TAMs. TAMs can also phagocytose dead tumor cells and enable antigen cross-presentation by DCs. Altering the functional state of TAMs may be preferred over their depletion to enhance intratumoral CTL activity.

Comparative transcriptome analysis of cell populations from the irradiated and the nonirradiated tumors in the same mice revealed that a 'CTL-permissive' TME was associated mostly with changes in CTL-extrinsic, rather than CTL-intrinsic gene signatures. We did not identify gene sets within the CTLs that could explain enhanced efficacy in the irradiated tumor. This indicates that the intrinsic quality of the CTLs that infiltrated the irradiated and nonirradiated tumor after RIT is similar and of good quality, which we also validated by *ex vivo* flow cytometry. Differentially expressed genes identified in the CTLs were associated with negative regulation of cytokine production and included *Foxp3* and *Il10.* We speculate that this is an immune regulatory signature that arose in CTLs that experienced and survived RT. It is unlikely that this population contributed to enhanced tumor control. Instead, our data suggest that CTL-extrinsic parameters (an altered TME) were decisive for CTL efficacy in the irradiated tumor after RIT. The differentially expressed genes only allow speculation regarding the mechanisms involved. Increased vasculogenesis identified in the irradiated tumor did not alter CTL infiltration into the irradiated tumor as compared with the nonirradiated tumor, as measured 8 days after RIT. Reduced proliferation of the tumor cells might have improved CTL-mediated tumor cell death by allowing T cells more time to complete killing. Potential sensitization of tumor cells to apoptosis by upregulation of *Bax* may have contributed to increased CTL-mediated tumor control in the irradiated tumor. RNA- and ribosome-associated processes were upregulated in irradiated tumor/stromal cells, suggestive of increased protein synthesis. RT enhances protein synthesis in an mTOR-dependent manner and increases peptide presentation by MHC and tumor cell immunogenicity[27]. We accordingly found that mTOR inhibition reduced the therapeutic efficacy of our RIT regimen[20]. Finally, processes that were altered nontranscriptionally may have allowed increased CTL efficacy in the irradiated tumor in our experimental setting.

In the rapidly developing RIT field, tumor cell destruction by RT is seen as a mode of vaccination, due to the release of antigens and 'danger' signals. Thus, the field emphasizes the potential of RT to contribute to CTL priming, which may result in systemic antitumor immunity and 'abscopal effects'

on nonirradiated tumor masses, when adequately supported by additional interventions[23,24,38]. RT may help to release danger-associated molecular patterns such as calreticulin or HMGB1 and/or cytosolic double-stranded DNA that can activate type I IFN signalling[24]. Such signals activate DCs from a 'tolerogenic' into an 'immunogenic' state[39]. In tumors that fail to deliver sufficient tumor antigens to DCs *de novo*, RT-induced debulking of the tumor could help to reach the 'antigen threshold' required for inducing a CTL response. Our study emphasizes that RT also modulates the TME to overcome T cell suppression. Combination of IT and RT may lead to regression of tumor masses outside of the field of radiation (e.g.[40,41]). However, to qualify systemic tumor regression as 'abscopal' effect of RT, it is required that RT also contributes to the systemic treatment effect, that is, synergistic with IT. Most likely, this can only be achieved when T cells are newly primed as a result of the combined treatment and exert their cytotoxic activity within the nonirradiated tumor.

We show that low-dose cisplatin can facilitate CTL activity in nonirradiated AT-3 tumors in mice treated with PD-1/CD137 targeting therapy, thereby functionally mimicking the immunomodulatory effects of RT. On the basis of our findings, 're-purposing' cisplatin at low-dose as an immunomodulatory drug may help to convert a CTL-suppressive TME into a CTL-permissive one. It will be of interest to test whether the immunomodulating effects of RT and cisplatin that are revealed here and their effective combination with CD137/PD-1 targeting therapy can also lead to increased and systemic antitumor effects in other mouse tumor models, such as the poorly immunogenic *MMTV-PyMT* breast cancer[42]. In general, our findings indicate that systemic tumor control may be achieved by combining IT protocols that promote T cell-priming with chemoradiation protocols that permit CTL activity in both the irradiated tumor and (occult) metastases.

Materials and Methods

Cells

AT-3 cells are derived from the MMTV-Polyoma virus middle-T (PyMT) transgenic mouse, back-crossed to C57BL/6[42] and were received from the Peter MacCallum Cancer Centre (Melbourne, Australia) in 2012. AT-3 cells were cultured in DMEM, supplemented with 10% fetal calf serum (FCS), 0.1 mmol/L nonessential amino acids, 1 mmol/L sodium pyruvate, 2 mmol/L L-glutamine, 10 mmol/L HEPES, and 30 μmol/Lβ-mercaptoethanol at 37°C, 10% CO_2. AT-3 cells were tested negative for *Mycoplasma* by PCR, and cells thawed from this 'master stock' were routinely used within 6 passages (approximately 3 weeks) for *in vitro* and *in vivo* experiments. PyMT protein expression in AT-3 cells was validated by Western blot analysis, but the cells were not further authenticated in the past year.

Mice

Six-eight-week-old female C57BL/6JRj (B6) mice were obtained from Janvier Laboratories (Le Genest Saint Isle, France) or from in-house breeding within the Netherlands Cancer Institute (NKI, Amsterdam, the Netherlands) and maintained in individually ventilated cages (Innovive) under specific pathogen-free conditions. All mouse experiments were performed in accordance with institutional and national guidelines and were approved by the Committee for Animal Experimentation at the NKI.

Therapeutic antibodies and reagents

Agonistic rat anti-mouse CD137 (clone 3H3, IgG2a)[43] was purified from hybridoma supernatant by affinity chromatography on protein-G. Rat anti-mouse PD-1 mAb (clone RMP1-14, IgG2a) and isotype control (2A3) were purchased from BioXCell. FTY720 was purchased from Cayman Chemical and cisplatin Pharmachemie BV (RVG 101430).

Tumor transplantation and therapy

AT-3 cell transplantation and therapy were performed essentially as described previously[19,20], with minor modifications. Briefly, mice were anesthetized with isoflurane, and injected with 1×10^6 AT-3 cells into the fourth mammary fat pad. In some experiments, mice were injected with 0.5×10^6 AT-3 cells into this fat pad on one side and with 2.5×10^6 AT-3 cells on the contralateral flank. The latter tumor was irradiated, and the other tumor served as the non-irradiated 'abscopal' tumor. Tumor size was measured using a caliper, and treatment was initiated when the tumors reached 20-25mm^2. Therapy was done with n=5-10 mice per group. RT was applied using an XRAD225-Cx system (Precision X-Ray), as described previously[20,34]. In brief, the mice were anesthetized with

isoflurane and a cone-beam CT scan of the mice was performed. The tumor(s) were localized on the CT scan and targeted with RT at 0.1-mm precision using round collimators 1.0 or 1.5 cm in diameter. A single fraction of 10-12 Gy (225 peak kilovoltage (kVp), filtered with 0.3 mm of copper (3 Gy/minute) was delivered. Control mice were anesthetized and underwent a cone-beam CT scan, but were not exposed to RT. Immunomodulatory mAbs toPD-1 and CD137 or an isotype control mAb were diluted in PBS. The antibodies were administered twice weekly for 2 weeks either intraperitoneally (PD-1 mAb, 100 µg per injection), or intratumorally (CD137 mAb, 25 µg in 10 µl per injection), with the first dose delivered immediately after RT treatment. For some experiments, cisplatin was administered intrave- nously at 4 mg/kg on day 0 (i.e., immediately after RIT) and on day 14. Tumor transplantation and therapy for RNAseq experiments was performed identically, with the exception that CD137 mAb was delivered i.p. (100 µg). The sphingosine-1-phosphate receptor-1 agonist FTY720 was diluted in saline (vehicle) and administered at 2 mg/kg by oral gavage. FTY720 treatment started one day prior to RT and was repeated three times per week throughout the duration of the experiment. All mice were sacrificed when the tumor(s) reached 100-200 mm^2. A tumor size of 100 mm^2 was set at a designated end point.

DNA vaccination

The DNA vaccination vector 'SIG-HELP-SNPTYSVM.KDEL' was generated by ligating annealed codon-optimized oligos (FW: 5'TCGAGAGCAACCCCACCTACAGCGTGATGAAGGACGAGCTGTAATAAT3' and RV: 5'CTAGATTATTACAGCTCGTCCTTCATCACGCTGTAGGTGGGGTTGCTC3') encoding SNPTYSVM.KDEL and *XhoI* and *XbaI* restriction sites in the *XhoI/XbaI* linearized pVax-HELP vector designed by Oosterhuis and colleagues[25], and described in detail by Ahrends and colleagues[33]. For DNA vaccination, the hair on a hind leg was removed using depilating cream (Veet; Reckitt Benckiser) on day -1. On days 0, 3 and 6, the mice were anesthetized with isoflurane, and 15 µl of a solution containing 2 mg/ml plasmid DNA in 10 mmol/L Tris and 1 mmol/L EDTA, pH 8.0, was applied to the hairless skin with a Permanent Make-up Up Tattoo machine (MT Derm GmbH), using a sterile disposable 9-needle bar with a needle depth of 1 mm and an oscillating frequency of 100 Hz for 45 seconds.

Flow cytometry

At the indicated time points, tumor-bearing mice were sacrificed, and tumor and lymphoid tissue were harvested. The tumors were mechanically chopped using a McIlwain tissue chopper (Mickle Laboratory Engineering) and a single-cell suspension was prepared by digesting the tissue in collagenase type A (Roche) and 25 µg/ml DNase (Sigma) in serum-free DMEM medium for 45 min at 37°C. Enzyme activity was neutralized by addition of DMEM containing 8% FCS, and the tissue was dispersed by passing through a 70-µm cell strainer. Single cells were first stained with PE- or APC-conjugated H-2K^b $PyMT_{246-253}$ (SNPTYSVM) tetramers for 15 min at 20°C in the dark. For

surface staining, cells were incubated with Fc receptor antibody (1:50, clone 2.4G2), followed by fluorochrome-conjugated antibodies (see below) for 30 min on ice in the dark in PBS containing 0.5% BSA and 0.01% sodium azide. Intracellular staining following restimulation with PMA and ionomycin was performed as described previously[20]. 7AAD (1:20; eBioscience) or Fixable Viability Dye eFluor 780 (1:1000; eBioscience), Zombie Red Fixable Viability Kit (1:5000, Biolegend) or DAPI (Invitrogen) was added to exclude dead cells. All experiments were analyzed using a BD LSRII, BD Fortessa or BD Symphony A5 flow cytometer with Diva software and the generated data were analyzed using FlowJo software.

Fluorochrome-conjugated mAbs with the following specificities were used for flow cytometry and obtained from BD Pharmingen unless otherwise specified: CD8-FITC (1:100, clone 56-6.7), CD4-eFluor450 (1:200, clone GK1.5), TCRβ-PECy5 (1:200; clone H57-597), CD43-PerCPCy5.5 (1:200, clone 1B11 (BioLegend, San Diego, CA)), CD45.2-eFluor605 (1:50; clone 30-F11), CD4-FITC (1:100, clone GK1.5), CD8-V450 (1:300, clone 56-6.7), CD11b-AF700 (1:200, clone M1/70), CD8-AF700 (1:200, clone 56-6.7), IFNγ-APC (1:100, clone XMG1.2), TNFα-PECy7 (1:200, clone MP6-XT22), CD4-BV711 (1:200, clone GK1.5), CD8α -PerCPCy5.5 (1:200, clone 56-6.7), CD3ε-PECy7 (1:50, clone 145-2C11), NK1.1-APC-eFluor780 (1:200, clone PK136), CD11b-BV786 (1:400, clone M1/70), FOXP3-APC (1:50, clone FJK-165), Ly6C-eFluor450 (1:400, clone HK1.4), Ly-6G-AF700 (1:200, clone 1A8), CD45-BUV395 (1:200, clone 3-F11), PE (1 µl/sample, clone PE001), I-A/I-E-AF700 (1:400, Clone M5/114.15.2, BioLegend), CD11c-PECy7 (1:200, clone HL3), XCR1-PerCPCy5.5 (1:200, Clone ZET, BioLegend), CD11b-BUV395 (1:50, Clone M1/70), CD45-BUV563 (1:200, clone 3-F11), CD45R/B220-eFluor450 (1:200, clone RA3-6B2), CD103-BV711 (1:50, clone M290), and F4/80-BV510 (1:50, clone BM8, BioLegend).

Within the live, single, $CD45^+$ cells, we gated and defined the cell populations as follows: $CD8^+$ T cells ($TCR\beta^+CD8^+$), $CD4^+$ T cells ($TCR\beta^+CD4^+$), Tumor-associated macrophages (TAMs, $F4/80^+MHCII^+$), Neutrophils ($Ly6G^+Ly6C^{int}$), inflammatory monocytes ($Ly6G^-Ly6C^{hi}$, as described in e.g.[44], NK cells ($NK1.1^+CD3^-$), NKT cells ($NK1.1^+CD3^+$), $CD103^+$ DCs ($F4/80^-CD11c^+MHCII^+CD103^+$), $CD11b^+$ DCs ($F4/80^-CD11c^+MHCII^+CD11b^+$).

Prediction of PyMT peptides and generation of PyMT-H-2K/D^b multimers

To identify AT-3 tumor antigens, we first used epitope prediction tools to define PyMT-derived peptides that could potentially bind to H-$2K^b$ and/or H-$2D^b$ MHC class I molecules. These peptides were then synthesized by the peptide facility at the NKI (Amsterdam, the Netherlands), and MHC tetramers were produced by UV-induced peptide exchange as described previously[45]. In brief, 28 peptides of PyMT (protein ID: NP_041265.1) predicted to bind either H-$2K^b$ or H-$2D^b$ (NetPan MHC 3.0 and NetPan MHC 4.0) were synthesized by the peptide facility at the NKI. These peptides were

individually exchanged into H-2K^b or H-2D^b molecules that had been refolded with a UV-sensitive peptide, allowing the generation of monomers with multiple specificities via a single reaction[45]. The resulting monomers were subsequently multimerized and conjugated to phycoerythrin (PE) or allophycocyanin (APC) and then used to screen for T -cell reactivity to MHC I-restricted PyMT epitopes using flow cytometry.

RNA preparation and sequencing

Using flow cytometry, CD43$^+$ CD8$^+$ T cells ('CTLs'), CD45$^+$ hematopoietic cells, and CD45$^-$ (tumor/stromal) cells were isolated from both the irradiated and non-irradiated tumors of 9 mice per experimental group, and material from 3 mice was pooled per sample to retrieve sufficient RNA. Cells were collected in RLT lysis buffer (QIAGEN) and total RNA was extracted using the RNAeasy mini kit (QIAGEN) in accordance with the manufacturer's instructions. The integrity of the total RNA was assessed using a 2100 Bioanalyzer System (Agilent). Only RNA samples with an RNA Integrity Number (RIN) $>$ 8 were used to create the library. Poly-A-selected RNA libraries were prepared using the TruSeq RNA library protocol (Illumina) and the resulting libraries were sequenced using an Illumina HiSeq2500 with V4 chemistry, with 50-bp single-end reads per lane.

Transcriptomics analysis of illumina sequencing data

Sequencing reads in FASTQ files were mapped to the mouse genome (build GRCm38.77) using Tophat v2.1[46], and the read summarization program HTseq-count[47] was used to count uniquely mapped reads against annotated genes. Differential expression analysis was performed using the DESeq2 package in R[48]. *P*-values were corrected for multiple comparisons, based on the False Discovery Rate (FDR), with significance considered at a *q*-value $<$0.01. Volcano plots were generated using ggplot2 (https://www.springer.com/gp/book/9780387981413).

Normalized read counts were used as input for Gene Ontology (GO) Gene Set Enrichment Analysis (GSEA) version 3.0[49,50] to identify groups of biological processes that were differentially expressed between cell populations obtained from the irradiated site and cell populations obtained from the nonirradiated site. We used the MSigDB C5 collection to identify enriched GO biological processes (BP). GSEA was performed with default parameters and gene set permutations were used. To gain a better overview of the linked biological processes, we generated enrichment maps using the Enrichment Map app v3.1.0, using cut-off values set at Q = 0.1 and Jaccard Overlap Combined = 0.375. We illustrated the largest gene set clusters and manually assigned the more general processes that these clusters represent.

The RNA-seq data reported in this paper have been deposited in the ArrayExpress database at EMBL-EBI (www.ebi.ac.uk/arrayexpress) under accession number E-MTAB-6914.

Immunohistochemical analysis

Harvested tumors were fixed for 24 h in ethanol (50%), acetic acid (5%), and formalin (3.7%), embedded in paraffin, and then sectioned randomly at 5 µm. The sections were then stained as described previously[34]. In brief, fixed sections were rehydrated and then incubated with primary antibodies to CD8 (eBioscience; clone 4SM15) and Foxp3 (eBioscience; clone FJK-16s). Endogenous peroxidases were blocked with 3% H_2O_2 and the sections were then incubated with biotin-conjugated secondary antibodies, followed by incubation with HRP-conjugated streptavidin-biotin (DAKO). The substrate was developed using diaminobenzidine (DAB; DAKO). We included negative controls to determine background staining, which was negligible. The stained sections were digitally processed using an Aperio ScanScope (Aperio) equipped with a 20x objective. ImageJ software was used to quantify the number of positive cells in 3-5 random fields of view (FOV) per slide.

Statistical Analysis

All summary data were analyzed using GraphPad Prism version 6 (GraphPad Software). Differences between various treatment groups were analyzed using the Mann-Whitney *U* Test. Differences in survival curves were analyzed using the Log Rank (Mantel-Cox) test. Differences with *P*-value <0.05 were considered statistically significant.

Disclosure of Potential Conflicts of Interest

No potential conflicts of interest were disclosed.

Authors' Contributions

Conception and design: P. Kroon, M. Verheij, J. Borst, I. Verbrugge Development of methodology: P. Kroon, T.N. Schumacher

Acquisition of data (provided animals, acquired and managed patients, provided facilities, etc.): P. Kroon, E. Frijlink, V. Iglesias-Guimarais, I. Verbrugge

Analysis and interpretation of data (e.g., statistical analysis, biostatistics, computational analysis): P. Kroon, E. Frijlink, V. Iglesias-Guimarais, A. Volkov, M.M. Van Buuren, J. Borst, I. Verbrugge

Writing, review, and/or revision of the manuscript: P. Kroon, E. Frijlink, A. Volkov, M.M. Van Buuren, M. Verheij, J. Borst, I. Verbrugge Administrative, technical, or material support (i.e., reporting or organizing data, constructing databases): P. Kroon, E. Frijlink

Study supervision: J. Borst, I. Verbrugge

Acknowledgments

We thank animal facility personnel for mouse husbandry, J.-J. Sonke and A. Khmelinskii for help in the small-animal radiotherapy facility, the Intervention Unit for help with the mouse experiments, R. Kerkhoven, A. Velds, M. Nieuwland, and I. de Rink of the genomics core facility for assistance and bioinformatics support with RNA sequencing, H. Yagita (Juntendo School of Medicine, Tokyo, Japan) for anti-CD137 (3H3), M. Toebes for assistance in generating tetramers, H. Hilkman and D. El Atmioui at the Peptide Production Facility for generating the peptides, J. Walker and N. Goense for technical assistance, K. de Visser and the Borst laboratory for helpful discussions, M. van den Broek for critical reading of the manuscript. Supported by the Dutch Cancer Society (grants NKI 2013-5951, 10764, to I. Verbrugge; 10894, to I. Verbrugge and J. Borst) and a Health Holland public-private partnership grant in collab- oration with Elekta (grant LSHM15036; to J.-J. Sonke).

References

1 Iwai, Y., Hamanishi, J., Chamoto, K. & Honjo, T. Cancer immunotherapies targeting the PD-1 signaling pathway. *Journal of biomedical science* **24**, 26 (2017).

2 Sharma, P., Hu-Lieskovan, S., Wargo, J. A. & Ribas, A. Primary, Adaptive, and Acquired Resistance to Cancer Immunotherapy. *Cell* **168**, 707-723 (2017).

3 Buchbinder, E. I. & Desai, A. CTLA-4 and PD-1 Pathways: Similarities, Differences, and Implications of Their Inhibition. *American journal of clinical oncology* **39**, 98-106 (2016).

4 Melssen, M. & Slingluff, C. L., Jr. Vaccines targeting helper T cells for cancer immunotherapy. *Current opinion in immunology* **47**, 85-92 (2017).

5 Chen, D. S. & Mellman, I. Oncology meets immunology: the cancer-immunity cycle. *Immunity* **39**, 1-10 (2013).

6 Spitzer, M. H. *et al.* Systemic Immunity Is Required for Effective Cancer Immunotherapy. *Cell* **168**, 487-502 e415 (2017).

7 Munn, D. H. & Bronte, V. Immune suppressive mechanisms in the tumor microenvironment. *Current opinion in immunology* **39**, 1-6 (2016).

8 Hui, E. *et al.* T cell costimulatory receptor CD28 is a primary target for PD-1-mediated inhibition. *Science* **355**, 1428-1433 (2017).

9 Krummel, M. F. & Allison, J. P. CD28 and CTLA-4 have opposing effects on the response of T cells to stimulation. *The Journal of experimental medicine* **182**, 459-465 (1995).

10 Wei, S. C. *et al.* Distinct Cellular Mechanisms Underlie Anti-CTLA-4 and Anti-PD-1 Checkpoint Blockade. *Cell* **170**, 1120-1133 e1117 (2017).

11 Kvistborg, P. *et al.* Anti-CTLA-4 therapy broadens the melanoma-reactive CD8+ T cell response. *Science translational medicine* **6**, 254ra128 (2014).

12 Sznol, M. *et al.* Pooled Analysis Safety Profile of Nivolumab and Ipilimumab Combination Therapy in Patients With Advanced Melanoma. *Journal of clinical oncology : official journal of the American Society of Clinical Oncology* **35**, 3815-3822 (2017).

13 Makkouk, A., Chester, C. & Kohrt, H. E. Rationale for anti-CD137 cancer immunotherapy. *European journal of cancer* **54**, 112-119 (2016).

14 Tolcher, A. W. *et al.* Phase Ib Study of Utomilumab (PF-05082566), a 4-1BB/CD137 Agonist, in Combination with Pembrolizumab (MK-3475) in Patients with Advanced Solid Tumors. *Clinical cancer research : an official journal of the American Association for Cancer Research* **23**, 5349-5357 (2017).

15 Bartkowiak, T. & Curran, M. A. 4-1BB Agonists: Multi-Potent Potentiators of Tumor Immunity. *Frontiers in oncology* **5**, 117 (2015).

16 Galluzzi, L., Buque, A., Kepp, O., Zitvogel, L. & Kroemer, G. Immunogenic cell death in cancer and infectious disease. *Nat Rev Immunol* **17**, 97-111 (2017).

17 Abuodeh, Y., Venkat, P. & Kim, S. Systematic review of case reports on the abscopal effect. *Curr Probl Cancer* **40**, 25-37 (2016).

18 van der Sluis, T. C. *et al.* Vaccine-induced tumor necrosis factor-producing T cells synergize with cisplatin to promote tumor cell death. *Clinical cancer research : an official journal of the American Association for Cancer Research* **21**, 781-794 (2015).

19 Verbrugge, I. *et al.* Radiotherapy increases the permissiveness of established mammary tumors to rejection by immunomodulatory antibodies. *Cancer Res* **72**, 3163-3174 (2012).

20 Verbrugge, I. *et al.* The curative outcome of radioimmunotherapy in a mouse breast cancer model relies on mTOR signaling. *Radiation research* **182**, 219-229 (2014).

21 Jones, A. T. *et al.* Characterization of the activation-associated isoform of CD43 on murine T lymphocytes. *Journal of immunology* **153**, 3426-3439 (1994).

22 Matloubian, M. *et al.* Lymphocyte egress from thymus and peripheral lymphoid organs is dependent on S1P receptor 1. *Nature* **427**, 355-360 (2004).

23 Dewan, M. Z. *et al.* Fractionated but not single-dose radiotherapy induces an immune-mediated abscopal effect when combined with anti-CTLA-4 antibody. *Clin Cancer Res* **15**, 5379-5388 (2009).

24 Vanpouille-Box, C. *et al.* DNA exonuclease Trex1 regulates radiotherapy-induced tumour immunogenicity. *Nat Commun* **8**, 15618 (2017).

25 Oosterhuis, K., Aleyd, E., Vrijland, K., Schumacher, T. N. & Haanen, J. B. Rational design of DNA vaccines for the induction of human papillomavirus type 16 E6- and E7-specific cytotoxic T-cell responses. *Human gene therapy* **23**, 1301-1312 (2012).

26 Coffelt, S. B., Wellenstein, M. D. & de Visser, K. E. Neutrophils in cancer: neutral no more. *Nature reviews. Cancer* **16**, 431-446 (2016).

27 Reits, E. A. *et al.* Radiation modulates the peptide repertoire, enhances MHC class I expression, and induces successful antitumor immunotherapy. *J Exp Med* **203**, 1259-1271 (2006).

28 Herbst, R. S. *et al.* Predictive correlates of response to the anti-PD-L1 antibody MPDL3280A in cancer patients. *Nature* **515**, 563-567 (2014).

29 Ayers, M. *et al.* IFN-gamma-related mRNA profile predicts clinical response to PD-1 blockade. *J Clin Invest* **127**, 2930-2940 (2017).

30 Futagawa, T. *et al.* Expression and function of 4-1BB and 4-1BB ligand on murine dendritic cells. *International immunology* **14**, 275-286 (2002).

31 Palazon, A. *et al.* The HIF-1alpha hypoxia response in tumor-infiltrating T lymphocytes induces functional CD137 (4-1BB) for immunotherapy. *Cancer discovery* **2**, 608-623 (2012).

32 Probst, H. C., McCoy, K., Okazaki, T., Honjo, T. & van den Broek, M. Resting dendritic cells induce peripheral CD8+ T cell tolerance through PD-1 and CTLA-4. *Nat Immunol* **6**, 280-286 (2005).

33 Ahrends, T. *et al.* CD27 Agonism Plus PD-1 Blockade Recapitulates CD4+ T-cell Help in Therapeutic Anticancer Vaccination. *Cancer Res* **76**, 2921-2931 (2016).

34 Kroon, P. *et al.* Concomitant targeting of programmed death-1 (PD-1) and CD137 improves the efficacy of radiotherapy in a mouse model of human BRAFV600-mutant melanoma. *Cancer immunology, immunotherapy : CII* **65**, 753-763 (2016).

35 Baruch, E. N., Berg, A. L., Besser, M. J., Schachter, J. & Markel, G. Adoptive T cell therapy: An overview of obstacles and opportunities. *Cancer* **123**, 2154-2162 (2017).

36 Dovedi, S. J. *et al.* Fractionated radiation therapy stimulates anti-tumor immunity mediated by both resident and infiltrating polyclonal T-cell populations when combined with PD1 blockade. *Clinical cancer research : an official journal of the American Association for Cancer Research* (2017).

37 Engelhardt, J. J. *et al.* Marginating dendritic cells of the tumor microenvironment cross-present tumor antigens and stably engage tumor-specific T cells. *Cancer cell* **21**, 402-417 (2012).

38 Rodriguez-Ruiz, M. E. *et al.* Abscopal Effects of Radiotherapy Are Enhanced by Combined Immunostimulatory mAbs and Are Dependent on CD8 T Cells and Crosspriming. *Cancer research* **76**, 5994-6005 (2016).

39 Gupta, A. *et al.* Radiotherapy promotes tumor-specific effector CD8+ T cells via dendritic cell activation. *J Immunol* **189**, 558-566 (2012).

40 Twyman-Saint Victor, C. *et al.* Radiation and dual checkpoint blockade activate non-redundant immune mechanisms in cancer. *Nature* **520**, 373-377 (2015).

41 Kwon, E. D. *et al.* Ipilimumab versus placebo after radiotherapy in patients with metastatic castration-resistant prostate cancer that had progressed after docetaxel chemotherapy (CA184-043): a multicentre, randomised, double-blind, phase 3 trial. *Lancet Oncol* **15**, 700-712 (2014).

42 Stewart, T. J. & Abrams, S. I. Altered immune function during long-term host-tumor interactions can be modulated to retard autochthonous neoplastic growth. *Journal of immunology* **179**, 2851-2859 (2007).

43 Shuford, W. W. *et al.* 4-1BB costimulatory signals preferentially induce CD8+ T cell proliferation and lead to the amplification in vivo of cytotoxic T cell responses. *The Journal of experimental medicine* **186**, 47-55 (1997).

44 Franklin, R. A. *et al.* The cellular and molecular origin of tumor-associated macrophages. *Science* **344**, 921-925 (2014).

45 Toebes, M. *et al.* Design and use of conditional MHC class I ligands. *Nature medicine* **12**, 246-251 (2006).

46 Trapnell, C., Pachter, L. & Salzberg, S. L. TopHat: discovering splice junctions with RNA-Seq. *Bioinformatics* **25**, 1105-1111 (2009).

47 Anders, S., Pyl, P. T. & Huber, W. HTSeq--a Python framework to work with high-throughput sequencing data. *Bioinformatics* **31**, 166-169 (2015).

48 Love, M. I., Huber, W. & Anders, S. Moderated estimation of fold change and dispersion for RNA-seq data with DESeq2. *Genome Biol* **15**, 550 (2014).

49 Subramanian, A. *et al.* Gene set enrichment analysis: a knowledge-based approach for interpreting genome-wide expression profiles. *Proceedings of the National Academy of Sciences of the United States of America* **102**, 15545-15550 (2005).

50 Mootha, V. K. *et al.* PGC-1alpha-responsive genes involved in oxidative phosphorylation are coordinately downregulated in human diabetes. *Nat Genet* **34**, 267-273 (2003).

Supplementary Data

Table S1 can be accessed under the following link:

https://aacrjournals.org/cancerimmunolres/article/7/4/670/469504/Radiotherapy-and-Cisplatin-Increase-Immunotherapy

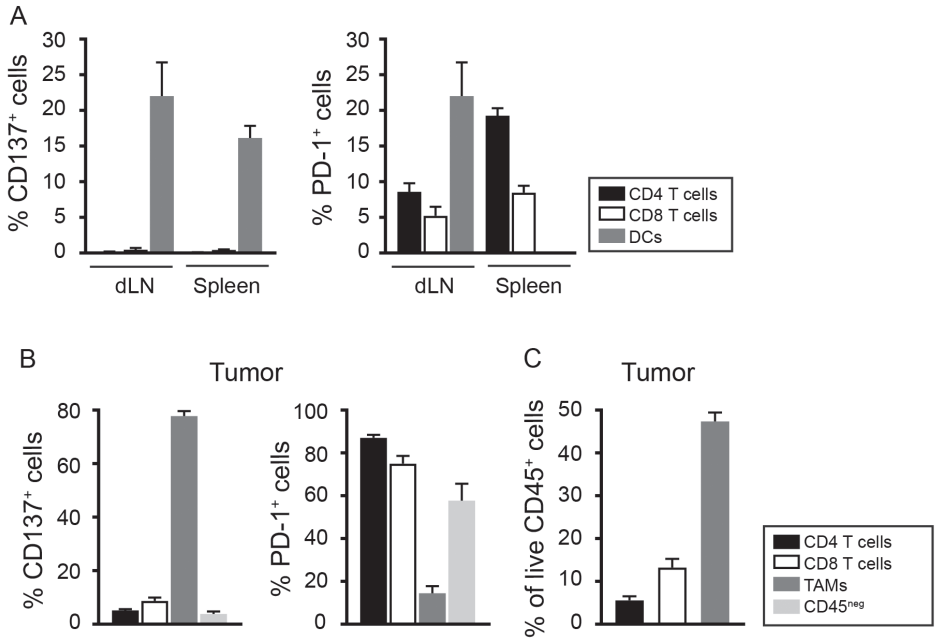

Figure S1. Related to Figure 1. Expression of the immunotherapy targets CD137 and PD-1 in AT-3 tumor-bearing mice. AT-3 tumor-bearing mice (n=3) were sacrificed, and the indicated tissues were harvested. (**A**) Percentage CD137$^+$ and PD-1$^+$ cells in the CD4$^+$ T (TCRβ$^+$ CD4$^+$), CD8$^+$ T (TCRβ$^+$ CD8$^+$), and dendritic cell (DC; CD11c$^+$MHCII$^+$) populations measured in the tumor draining lymph node (dLN) and spleen. (**B**) Percentage of CD137$^+$ and PD-1$^+$ cells in the indicated cell populations isolated from the tumor tissue. TAMs; tumor-associated macrophages. (**C**) Percentage of CD4$^+$, CD8$^+$ T cells and TAMs within the CD45$^+$ population isolated from the tumor tissue.

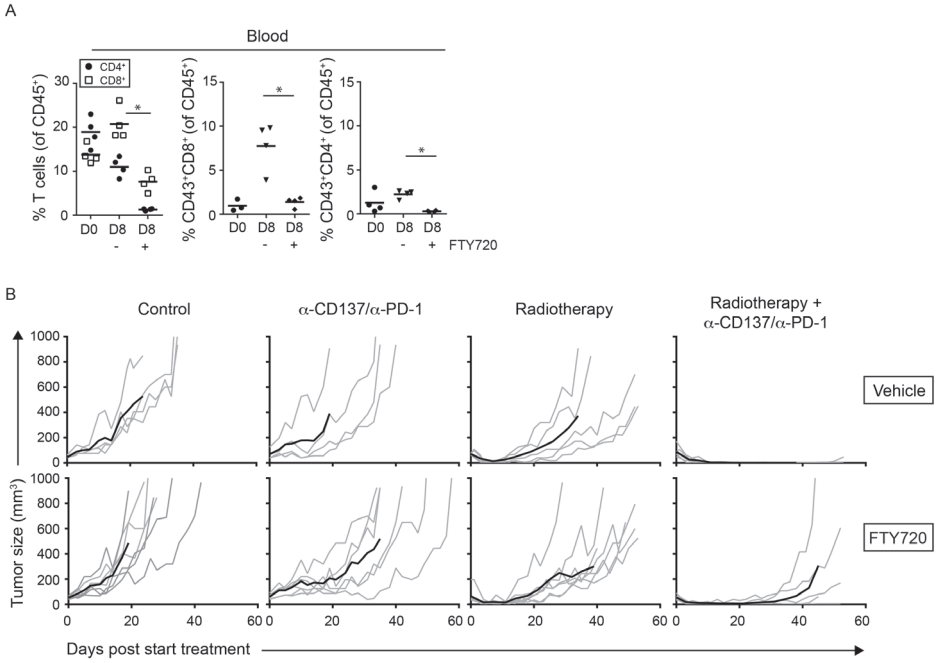

Figure S2. Related to Figure 2. Depletion of effector phenotype T cells from the circulation following RIT combined with FTY720 treatment.

(**A**) Mice (3-4 per group) bearing an established AT-3 tumor (>20mm^2) received either saline of FTY720 3x weekly in combination with RIT (see Figure **2A** for the experimental set-up). The percentage of the (CD43$^+$) CD4$^+$ and CD8$^+$ T cells within the CD45$^+$ population was measured in the blood before (D0) or 8 days after (D8) the start of RIT. (**B**) Tumor growth curves of the AT-3 tumor-bearing mice (4-5 per group) receiving radiotherapy (10 Gy), immunotherapy (α-CD137/α-PD-1 mAbs) alone or in combination or mock-treatment, in presence or absence of FTY720; grey lines: individual tumor growth curves, black lines: average of the group.

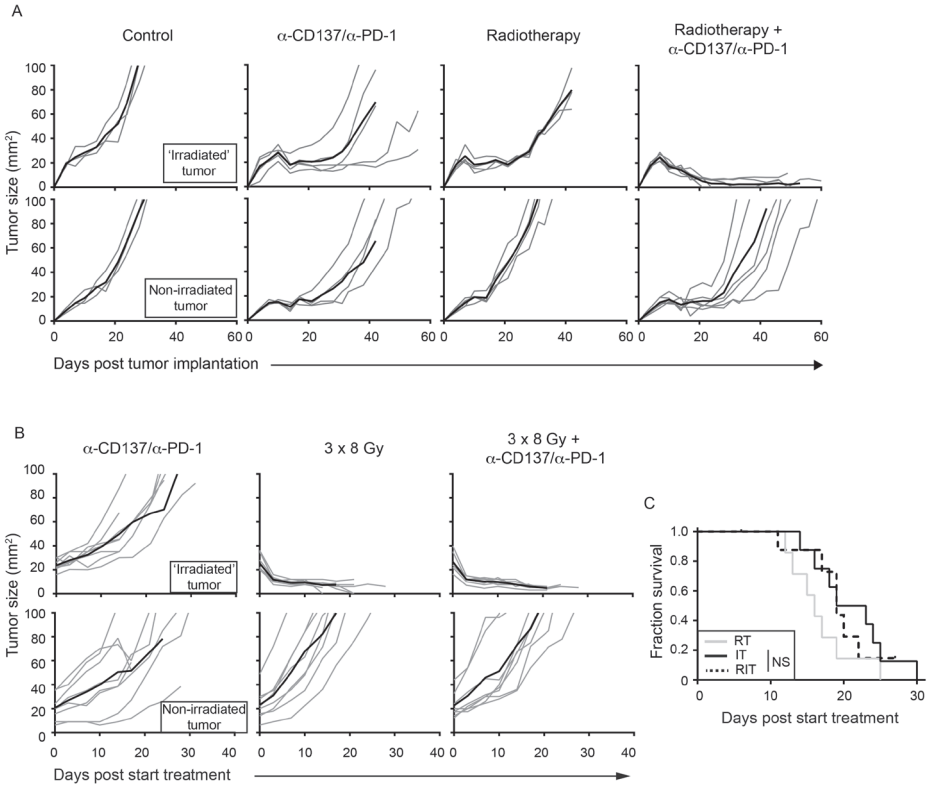

Figure S3. Related to Figure 3. Time course of tumor size following radio-immunotherapy delivered as one dose or in 3x 8 Gy fractions.
(**A** and **B**) Time course of tumor size in mice treated as indicated. In each plot, the gray and black lines represent individual tumors and the mean of the group, respectively. (**C**) Survival curve of mice bearing bilateral AT-3 tumors, treated radiotherapy (RT: 3x 8 Gy) alone, immunotherapy alone (IT), or both RT and IT (RIT).

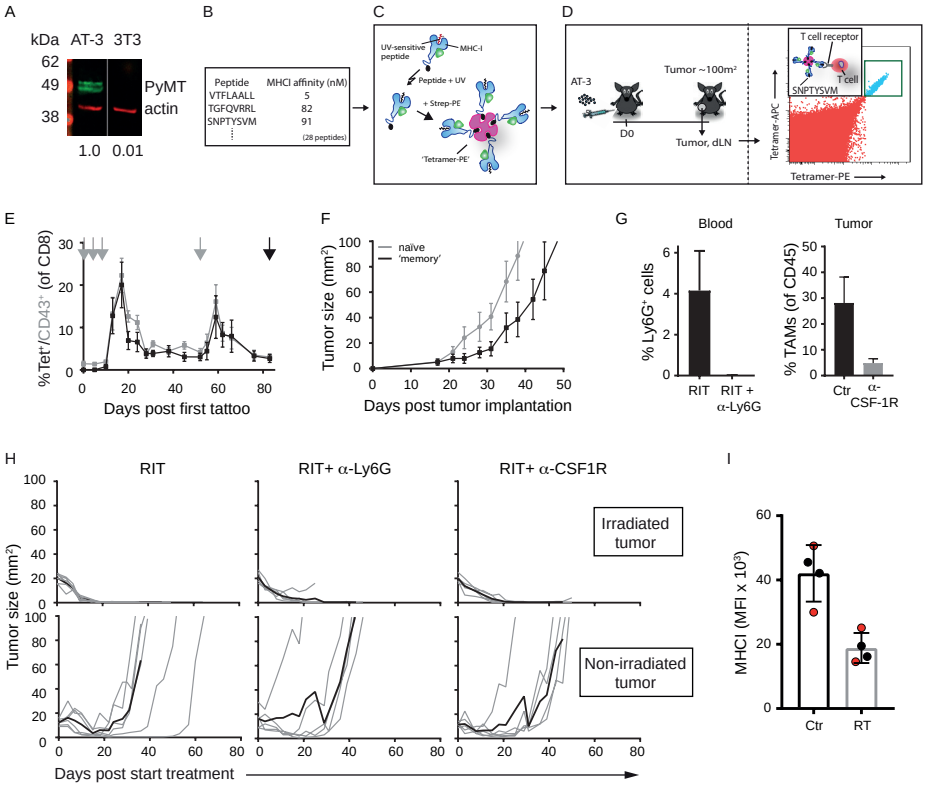

Figure S4. Related to Figure 4. Identification of an AT-3 tumor specific (CD8) T cell epitope, and targeting either Ly6G or CSF1R does not improve RIT-mediated control of non-irradiated tumor.
(**A**) PyMT and actin immunoblot AT-3 or 3T3 cell lysates. Note that the elft and right lanes are from the same blot and the relative PyMT expression levels are shown below the image. (**B**) A total of 28 PyMT peptides that are predicted to bind to MHC-I with the indicated affinity were synthesized; note that only the three peptides with the highest affinity are shown. (**C**) Peptide-MHC multimers ("tetramers") were generated for the 28 peptides as shown. (**D**) $CD8^+$ T cells from the AT-3 tumor and dLN were analyzed for tetramer-binding, indentifying SNPTYSVM as a tumor antigen. (**E-F**; related to Figure **4A-D**) Mice (6 per group) received SNPTYSVM vaccination (for details see Figure **4A**) on days 0,3, 6 and 52 (gray symbols). On day 83 (the black arrow), the mice were implanted with AT-3 tumor cells. (**F**) Time course of the tumor size of "memory" mice (i.e. the mice shown in Figure **S4E** that received DNA vaccination at the times indicated by the black arrow), and age-matched naïve mice (shown in gray lines) after implantation with $2x10^5$ AT-3 tumor cells in the fourh mammary fat pad. (**G**; related to Figure **4G**) Percentage of $Ly6G^+$ (left) and TAMs (rigt) measured in the blood and tumor tissue of mice treated with RIT in the absence or presence of anti-Ly6G or anti-CSF-1R mAbs. (**H**) Time course of the size of the irradiated an non-irradiated tumors in the mice treated as indicated. The gray and black lines repesent individual and average data, respetively, for the mice shown in Figure **4G**. (**I**) MHC I expression on tumor/stromal cells ($CD45^+$) from mice beraing irradiated (10:37 PM) and non-irradiated (Ctr) AT-3 tymors. Data shown is from Day 3 (red circles) and Day 8 (black circles) after treatment (2 mice per timepoint).

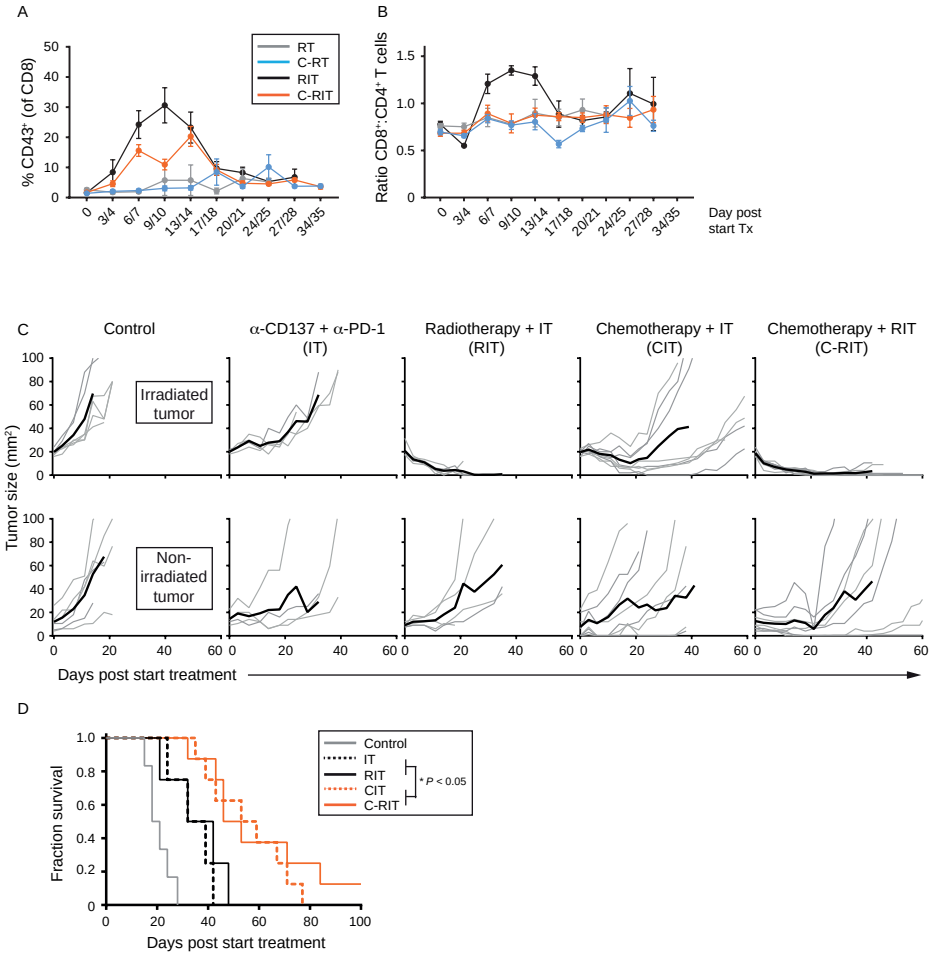

Figure S5. Related to Figure 6. Cisplatin modestly reduces the RIT-induced increase in CD8:CD4 T cell ratio and enhances (R)IT-medated control of non-irradiated tumors.
Peripheral blood collected from the same mice shown in Figure **6B,C** were analyzed for the percentage of $CD43^+$ cells within the $CD8^+$ T cell population (**A**) and the $CD8^+$:$CD4^+$ T cell ratio (**B**) on the indicated days. (**C**) Individual (grey lines) and average (black line) tumor growth curves and (**D**) survival curves of mice treated with the indicated therapies.